Long-range transport of littoral methane explains the metalimnetic methane peak in a large lake

Santona Khatun[1]*, Jasmine S. Berg[1], Didier Jézéquel[2], Marthe Moiron[3], Nicolas Escoffier[1], Carsten Schubert[4,5], Damien Bouffard[1,4], Marie-Elodie Perga[1]

[1]Faculty of Geosciences and Environment, Institute of Earth Surface Dynamics, University of Lausanne, 1015 Lausanne, Switzerland

[2]Institut National de Recherche pour l'Agriculture, l'Alimentation et l'Environnement (INRAE), UMR CARRTEL, 74200 Thonon-les-Bains, France & IPGP-Univ. Paris Cité, 75238 Paris Cedex 05, France

[3]Sciences et Techniques de l'Environnement (S.T.E.), 73372 Le Bourget du Lac cedex, France

[4]Eawag, Swiss Federal Institute of Aquatic Science and Technology, Department of Surface Waters - Research and Management, 6047 Kastanienbaum, Switzerland

[5]Institute of Biogeochemistry and Pollutant Dynamics, ETH Zurich, 8092 Zurich, Switzerland

*Corresponding author: santona.khatun@unil.ch

Keywords: Methane, freshwater ecosystem, turbidity, large lake, interflow, isotopy

Abstract

In large and stratified lakes, substantial methane stocks are often observed within the metalimnion. The origin of the methane (CH_4) accumulated in the metalimnion during stratification, which can sustain significant emissions during convective mixing, is still widely debated. While commonly attributed to the transport of methane produced anaerobically ex-situ, recent evidence suggests that oxic in situ methane production could also contribute to metalimnetic methane peaks. Here, we assessed the origin, *i.e.*, pelagic CH_4 production or transport of sublittoral CH_4 through the interflow, of metalimnetic methane in Lake Geneva, the largest lake in Western Europe. Microbial diversity data do not support the hypothesis of oxic methane production in the metalimnion. In contrast, both spatial and temporal surveys of methane show that maxima occur at depths and sites most affected by the Rhône River inflow. Methane $\delta^{13}C$ values point to an anaerobic sublittoral methane source, within a biogeochemical hotspot close to the river delta region, and an efficient transport across several kilometers in a vertically well-constrained metalimnion. Our current findings emphasize the indirect role of river interflows for the long-range transport of CH_4 produced in sediment biogeochemical hotspots, even for large lakes where sublittoral habitats represent a fairly limited fraction of the lake volume.

Introduction

Methane (CH_4) is a potent greenhouse gas, whose atmospheric increase is responsible for 16-25% of atmospheric warming to date (IPCC 2021). Aquatic ecosystems contribute half of the global methane emissions, 34% of which come from freshwater lakes (Rosentreter et al. 2021). Lake CH_4 emissions are also expected to increase due to eutrophication, urbanization, and warming, creating a positive climate feedback (Saunois et al. 2016). Nonetheless, the mechanisms underlying methane supersaturation in lakes and leading to net CH_4 emissions remain debated.

There are different metabolic pathways by which CH_4 can be produced in aquatic environments. CH_4 is a byproduct of organic matter decomposition under anoxic conditions and acetoclastic or hydrogenotrophic methanogenesis in stagnant waters and anoxic sediments is an important contributor to the lake CH_4 (Rudd and Hamilton 1978; Bastviken et al. 2004; Conrad et al. 2020). Recent discoveries have yet brought to light alternative metabolic pathways by which organisms, especially primary producers, can produce CH_4 in oxic conditions (Khatun et al. 2019; Günthel et al. 2019; Ernst et al. 2022; Hilt et al. 2022). The current debate revolves around the relative contribution of both processes to the actual CH_4 emissions from lakes (Encinas Fernández et al. 2016; Donis et al. 2017; Günthel et al. 2019; Peeters and Hofmann 2021).

Diffusive CH_4 fluxes between lakes and the atmosphere are directly proportional to the gradient of concentrations between the atmosphere and the surface mixed layer. The concentration of CH_4 in the surface mixed layer is also strongly tied to lake morphology, decreasing with the ratio of shallow water surface area to total lake area (Encinas Fernández et al. 2016). Therefore, CH_4 concentrations in the surface mixed layer of large, deep stratified lakes can be above saturation but generally lower than in shallow lakes (Encinas Fernández et

al. 2016) and pelagic CH_4 emissions are thus expected to be limited (Li et al. 2020). In such lakes, the greatest CH_4 concentrations are typically observed in the metalimnion, where the water stability is the greatest (Donis et al. 2017; Schroll et al. 2023). Nonetheless, part of the CH_4 accumulated in the metalimnion can diffuse to the atmosphere when the thermocline deepens due to convective mixing, either during sudden storm events or seasonal lake overturns (Zimmermann et al. 2022; Michmerhuizen et al. 1996; Riera et al. 1999). Therefore, metalimnetic CH_4 may ultimately contribute to the total annual emissions of deep lakes. Previous evidence suggested that the accumulation of methane in the surface mixed layer and in the metalimnion can originate from different sources and be driven by different mechanisms (Donis et al. 2017).

The metalimnetic CH_4 peaks observed in deep stratified lakes have been predominantly attributed to a physical accumulation of methane from distant methane production zones of the lake, *i.e.*, anoxic deep layers, deep and sublittoral sediments (Donis et al. 2017; Kang et al. 2024) or even river-borne methane (Murase et al. 2003, 2005; Tsunogai et al. 2020). Methane produced inshore or in deeper layers diffuses to the metalimnion, where the high water mass stability limits further upward diffusion (Encinas Fernández et al. 2016; Donis et al. 2017; Peeters and Hofmann 2021). However, several studies have pointed out that physical accumulation may not be the sole process at play.

In situ pathways of oxic CH_4 production (OMP) can also sustain metalimnetic CH_4 peaks in stratified lakes (Yao et al. 2016; Wang et al. 2021; Schroll et al. 2023). Planktonic microorganisms, including cyanobacteria, have been shown to produce methane in situ and in vitro under oxic conditions (Bižić et al. 2020). In clear, stratified lakes, metalimnetic CH_4 maxima are often correlated with oxygen supersaturation and deep chlorophyll maxima in the thermocline in summer (Grossart et al. 2011; Tang et al. 2016). Several aerobic methanogenic

pathways have been proposed through the metabolism of methylated compounds or phosphonate under nutrient-depleted conditions (Bižić-Ionescu et al. 2018; Khatun et al. 2019; Perez-Coronel and Michael Beman 2022). For instance, methylphosphonate metabolism was shown to contribute to the CH_4 metalimnetic peak of Lake Yellowstone (Wang et al. 2017). In two German stratified lakes, methylphosphonate, methylamine, and methionine acted as potent precursors of CH_4, at least partly sustaining the metalimnetic CH_4 peak (Schroll et al. 2023). The relative share of transport and accumulation versus in situ production in the dynamics of the metalimnetic methane peaks of observed in large and deep lakes therefore deserves further investigation.

Lake Geneva is a large and deep lake where a metalimnetic methane peak has been sporadically observed (Donis et al. 2017). While the cause of the seasonal metalimnetic methane in Lake Geneva remains unknown, both OMP and lateral transport of littoral CH_4 are likely to co-occur (the lake hypolimnion is mostly oxic and methane production in deep sediment is rather limited). On the one hand, phosphate limitation in the photic layer in summer and the presence of polyphosphate nodules in cyanobacterial cells of Lake Geneva (N Escoffier, pers. comm.) pinpoints the potential for OMP through phosphonate decomposition (Yao et al. 2016; Wang et al. 2017, 2021). On the other hand, transport in the metalimnion is efficient and long-ranging during the stratified periods, as evidenced by the persistent Rhône River (the main inflow) signature (isotopically and through turbidity) up to 30 kilometers away from the river mouth (Ishiguro and Balvay 2003; Halder et al. 2013). The riverine water is initially trapped as an interflow in the thermocline also known as metalimnetic intrusions of river plumes during stratification (Giovanoli & Lambert 1985; Piton et al. 2022) and then transported by the basin-scale internal seiches and large-scale gyres which mostly follow the northern shore (Hasegawa-Ishiguro & Okubo 2008; Cimatoribus et al. 2019; Nouchi et al. 2019). Such a river interflow is a significant conveyor of nutrients, dissolved oxygen, and

turbidity across the lake (Giovanoli & Lambert 1985; Escoffier et al. 2022). The sublittoral zone of the Rhône lacustrine delta has previously been shown to emit CH_4 through sediment diffusion and bubbling (Sollberger et al. 2014). We hypothesize that the metalimnetic transport of CH_4 produced in the proximal Rhône delta could also sustain the offshore metalimnetic peak. Our main objective is thus to measure the dynamics of the metalimnetic CH_4 peak in Lake Geneva and to determine whether aerobically in situ-produced by pelagic microbes or littoral-transported methane is the main contributor to the metalimnetic CH_4 peak.

Material and Methods

Site Description:

Lake Geneva is a temperate mono-oligomictic lake at the border of Switzerland and France (Fig. 1). Most of the catchment area (7,395 km^2) lies in the Swiss Alps, and, to a minor extent, in the French Alps and Jura mountains. Lake Geneva has a maximum depth of 309 m, with a surface area of 581 km^2 and a mean water retention time of 11.4 years. The lake is oligo-mesotrophic (TP = 17 $\mu gP.L^{-1}$, CIPEL 2019). Lake Geneva is strongly stratified from early May to early October with a thermocline depth close to 20 m in summer (Michalski and Lemmin 1995). The main tributary of Lake Geneva is the Rhône River, a glacial river flowing from the Swiss Alps, which discharges 70% of the total water inputs, nutrients, and sediment to the north-eastern part of the lake (Fig. 1). Due to its glacial regime, the Rhône River's maximal discharge occurs in June-August, with relatively cold (temperature ranging from 9-10°C), low conductivity (150-230 $\mu S.cm^{-1}$) sediment-laden meltwater (turbidity in 400-500 FTU) (Nouchi et al. 2019). The Rhône water flowing in the summer is of relatively higher density than the lake surface waters and, at its inflow, sinks downslope along the lakebed until it reaches the depth where the river and lake water densities are equal. In summer, this depth of equal density occurs at the thermocline, resulting in Rhône water intrusion as an interflow

(Stevens et al. 1995; Ahlfeld et al. 2003). Because of the water's glacial origin, the propagation of the interflow within Lake Geneva can be tracked by the turbidity maximum and conductivity minimum in the water column (Escoffier et al., 2022). When the lake is strongly stratified, the interflow is trapped in the thermocline and loses its momentum within a few kilometers before being controlled by lake dynamics (Giovanoli 1990, Cimatoribus et al. 2019; Piton et al. 2022) with a typical counterclockwise circulation pattern (Bouffard and Lemmin 2013) and gyre structures as a response of wind forcing (Cimatoribus et al. 2019).

Water samplings:

We mainly sampled Lake Geneva during the stratified seasons (from July to October) of the years 2021 and 2022 for both the temporal and spatial dynamics of the metalimnetic methane peak (Fig. 1 and Table S1). We collected water samples for dissolved methane measurement at 15 stations near the Rhône River delta on July 22-23, 2021 (Fig. 1a). Stations 1-7 were within 1km of the shore or river mouth, and at depths < 100 m, and may qualify as littoral or sublittoral zones. Stations 8-15, were > 135 m deep, and further than 1 km from the closest shore. The Rhône River was also sampled for methane concentrations a few km upstream from the river mouth (Rhône Porte du Scex station) on five dates from March to September 2021 (Table S1). In 2021 and 2022, the temporal dynamics of metalimnetic methane were surveyed at a fixed point, *i.e.*, the LéXPLORE platform (depth 110 m, Fig. 1b), a high-tech floating laboratory on Lake Geneva (Wüest et al. 2021, https://lexplore.info/fr/accueil/), anchored 600 m away from the shore. We sampled there six times in the summer of 2021 (*i.e.*, April 7, May 10, May 31, July 5, July 26, and September 30) and three times in 2022 (*i.e.*, July 27, September 23, and October 13). To test a potential link between the methane dynamics at the Rhône River mouth and the temporal dynamics at LéXPLORE, the samplings of 2022 were completed by a spatial survey along the main direction of the Rhône interflow

(Fig. 1c): five pelagic (>100 m depth) sampling stations (StaA-StaE) along the North-eastern branch of the Rhône interflow were sampled on September 23, 2022, starting from the interflow of the Rhône River (about 0.3 km downstream from the mouth of the river) towards the LéXPLORE station (about 19 km from the mouth of the river).

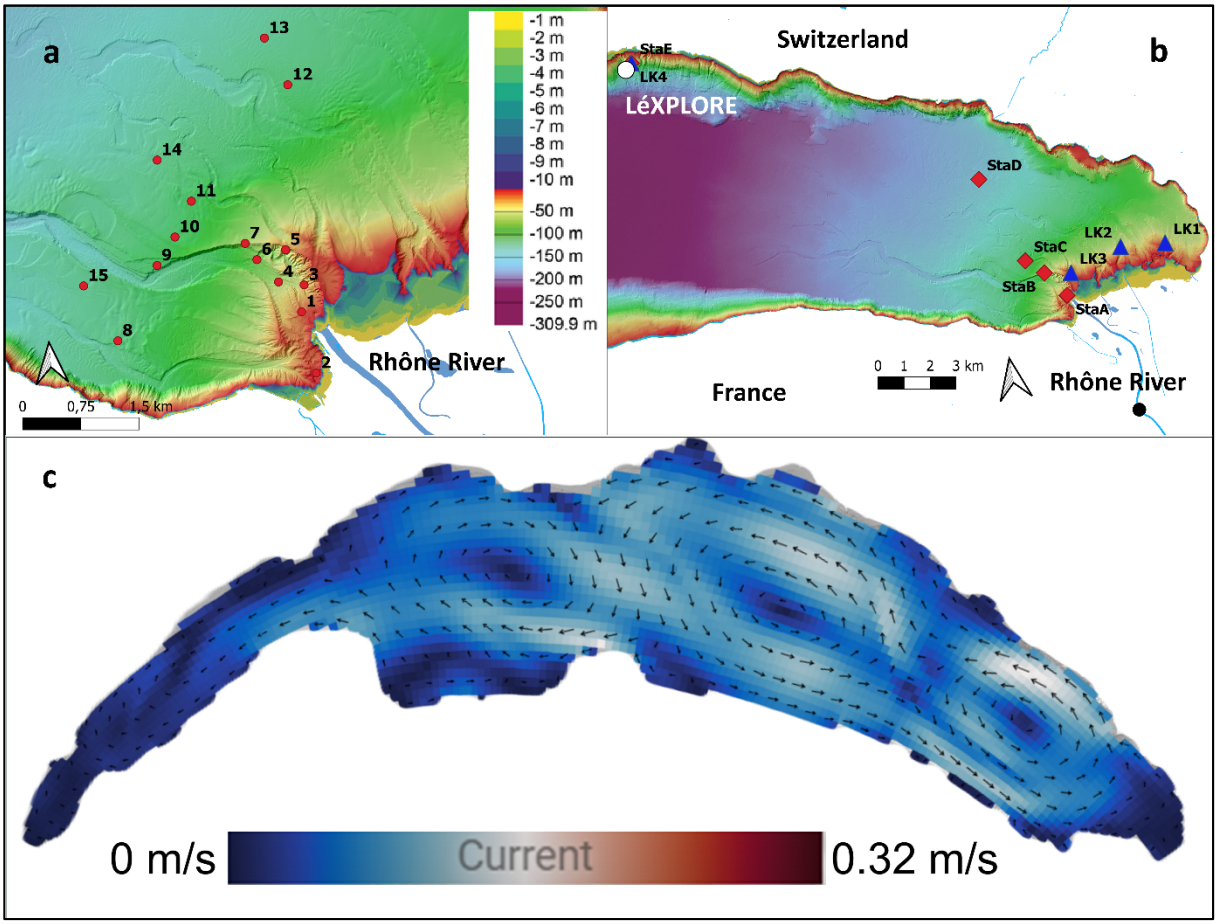

Fig. 1 Geographic location of the sampling stations in Lake Geneva. (a) The red dots indicate the 15 water sampling stations near the Rhône River delta in 2021. **(b)** The white and black dots respectively represent the LéXPLORE platform for the water sampling stations in July-October, 2021-2022 and the Rhône River water sampling in March- September 2021. The red diamonds and blue triangles indicate five water sampling stations in September 2022 (StaA-StaE) and four sediment sampling stations in July 2023 (LK1-LK4), respectively. **(c)** The modelled velocity of water at the 10m depths of the Rhône interflow in Lake Geneva is shown

for the period of the water sampling on September 23, 2022. Model outputs can be found on Alplakes.eawag.ch which baseline is described in Baracchini et al (2020). The sampling station coordinates are listed in the supplementary table (Table S1).

Physicochemical parameters at each sampling station were measured using vertical profiling with a CTD (Conductivity, Temperature, and Depth) probes at the LéXPLORE platform (OCEAN SEVEN 316Plus, IDRONAUT Srl) or by deploying the EXO2 multiparameter sonde (YSI, Xylem Inc., Yellow Springs, OH) from a boat. These probes were used to measure temperature, dissolved oxygen (DO), turbidity, conductivity, blue-green algae, and chlorophyll (Chl *a*) concentration. Physico-chemical properties at LéXPLORE could be complemented with monitoring data retrieved from the Datalakes web-based open platform (https://www.datalakes-eawag.ch/). To quantify the strength of the stratification in the water column, a squared buoyancy frequency or Brunt–Väisälä frequency (N^2) was calculated using the pressure, salinity, and temperature data. The equation is as follows:

$$N^2 = \frac{-g}{\rho}\left(\frac{\partial \rho}{\partial z}\right) \; ; \; s^{-2}$$

Here, ρ and g are the density and earth's gravitational acceleration, respectively. The change in density with depth ($\frac{\partial \rho}{\partial z}$) was calculated following Fofonoff and Millard (1983).

Water sampling depths were selected based on temperature profiles as well as Chl *a* and turbidity peaks. Two to four water samples were collected per depth for all stations using a 5 L Niskin bottle. Water was dispensed from the Niskin into pre-weighed 60 mL glass serum vials and preserved with $CuCl_2$ or NaOH for methane quantification in both 2021-2022 and isotopic measurements only in 2022 (Rudd and Hamilton 1978). The vials were immediately

capped with gas-tight butyl rubber stoppers and sealed with aluminum crimp caps leaving no headspace. Bottles were stored in the fridge at 6°C.

Water samples for microbial analysis in 2022 were pre-filtered with a 150-µm mesh to remove the large planktonic organisms (Table S1). For Chl *a* measurement, around 500-1000 mL of lake water was filtered with GF/F filters and stored at −20°C. Chl *a* was extracted spectrophotometrically according to Talling and Diver, 1963. Microbial samples for DNA analyses were collected by filtering 1-2 L of lake water for each depth on 0.22 µm filters (Sterivex filter cartridges, Millipore, Billerica, MA, USA) and stored at −20°C until further analysis.

Sediment sampling:

Sublittoral sediment samples were collected to obtain an isotopic endmember for sublittoral methane. Sediment samples (approximately 25-50 m, sampling depths 0 - 15 cm) were collected at four stations of Lake Geneva on July 26-27, 2023 (Fig. 1 and Table S1). Among them, three stations were from the littoral sediments near the Rhône River delta, and one station was near the LéXPLORE platform. Cut-off syringes were inserted into the holes of pre-drilled core liners with a resolution of 5 cm and about 2 mL of sediment was transferred directly into serum vials (100 ml) pre-filled with NaOH solutions following the protocol of Sobek et al. 2009 (Sobek et al. 2009). The vials were capped with gas-tight butyl rubber stoppers and sealed with aluminum crimp caps.

Methane and isotopic analysis:

For samples collected before September 2021, methane was detected on board using an equilibration technique coupled to a Contros HydroC™ CH_4 (GmbH, Germany) equipped with a High-Sensitive Methane Sensor (HISEM) based on a Tunable diode laser absorption spectroscopy (TDLAS). The sensor had a resolution of ± 0.1 ppm and an accuracy of ± 0.5 ppm. The probe was pre-calibrated using two CH_4 standards obtained from GazDetect™ (100.7 and 1013 ppm) and N_2 AlphaGas as a zero standard. A 2 L Duran bottle was filled completely with water and closed with a two-inlet cap equipped with a short tube and a long tube ending in a gas diffuser (aquarium type). N_2 gas was pumped through the short tube to replace the water above the 2L mark and generate an N_2 headspace. The calibration gases were bubbled through the gas diffuser and exited through the top of the bottle towards the CH_4 sensor. After passing through the sensor, gas recirculated through the bottle creating a gas loop with an equilibration time of 5 to 6 min. The temperature of the 2 L sample was measured during the equilibration process along with the headspace CH_4 concentration.

Samples collected in September 2021 (60 mL glass serum vials) were preserved with $CuCl_2$ until measurement on a gas chromatograph GC 2010 Shimadzu (equipped with Flame ionized detector-FID, Germany). The limit of detection was less than 1 ppm for methane measurement. In 2022, all the samples for both methane concentrations and isotopic measurements were preserved with NaOH. Dissolved CH_4 was extracted using the headspace (Nitrogen gas) displacement method and measured by a Gas Chromatograph (Joint Analytical Systems, Germany) equipped with a FID (Column: Supelco Carboxen-1010 PLOT, split-less injection at 200°C, and detection at 350°C temperature, CH_4 detection limit of less than 1 ppm) housed by the Swiss Federal Institute of Aquatic Science and Technology, Department of Surface Waters - Research and Management, Kastanienbaum, Switzerland. Dissolved methane concentrations were calculated based on Henry's Law at standard conditions of 1013.25 mbar and 25°C.

The $\delta^{13}C$ CH_4 isotope analyses for water and sediment samples (2022-2023) were performed on a gas chromatograph combustion isotope ratio mass spectrometer (GCC-IRMS, Agilent Technologies 6890 N) with a trace gas coupled to an isotope ratio mass spectrometer (Thermo Finnigan, UK). The headspace gas samples (20-30 mL) were analyzed using the IonVantage software. Results are expressed using the δ notation relative to the Vienna Pee Dee belemnite (VPDB) standard with an analytical error below 1.1‰.

DNA extraction and 16S rRNA gene amplicon analysis:

Microbial biomass collected on Sterivex filters (0.22 µm, Millipore, Billerica, MA, USA) was processed using the PowerWater DNA Extraction Kit (Qiagen, Germany) according to the manufacturer's instructions. We amplified the V3 and V4 regions of the 16S rRNA gene to assess the total microbial taxonomic diversity in the collected samples. We also focused on two specific genes: the marker genes C-P lyase (*phnJ*) of bacteria associated with the OMP pathway by phosphonate decomposition (Wang et al. 2021) and the methyl coenzyme M reductase (*mcrA*) of methanogenic archaea, associated with acetoclastic methane production (anoxic methane production, Angel et al. 2011). The barcoded primer pairs are listed in Table S2. Polymerase chain reactions (PCR) were performed using the Taq PCR Core Kit (Qiagen, Germany). Each reaction contained 1 µL of template DNA, 0.5 µL of forward primer (0.5 µM), 0.5 µL of reverse primer (0.5 µM), 5 µL of 10x buffer (0.5x), 1 µL of dNTP mix (10 mM), 0.25 µL of Tag (1.25 units/reaction), 2 µL of $MgCl_2$ (15 mM), and 39.75 µL PCR grade sterile water. Thermocycling conditions for all primers are presented in Table S2. The PCR products were visualized by gel electrophoresis and successful amplicons of 16S rRNA gene, and *phnJ* gene were then sent for sequencing.

Gene sequencing and microbial community analysis:

Samples were sequenced and demultiplexed at the Lausanne Genomic Technologies Facility (LIMS), University of Lausanne, Switzerland on the Illumina MiSeq v3 flow cell for 600 cycles (for bacteria) with 300-nucleotide paired-end reads and Illumina NovaSeq 6000 for 300 cycles (for *phnJ*) with 150-nucleotide paired-end reads. The Illumina 16S Sequencing Library Preparation protocol is outlined by the LIMS. The sequences obtained from the LIMS were demultiplexed using the bcl2fastq2 Conversion Software (version 2.20, Illumina). The quality trimming parameters were used to remove primer sequences, low-quality bases, and low-quality reads (Table S2). Amplicon sequence variants (ASV) were generated, and the chimeras were removed by DADA2 (Callahan et al. 2016) to allow sufficient overlap for the merging of forward and reverse reads. ASVs were taxonomically annotated using the Silva (nr99/v138.1) database (Quast et al. 2012).

The final ASV counts were normalized as relative abundances (%). The 16S amplicon reads could be used as a proxy for the relative abundance of bacteria with 41,529–56,013 reads per sample. A total of 14,989–34,084 cyanobacteria amplicon reads and 4,62,442– 17,34,112 *phnJ* gene reads were recovered per sample. Further information on the selection of the *phnJ* gene is provided in Table S2.

Statistics and model selection:

Significant differences in biogeochemical properties between stations shown in box plots were assessed using the Kruskal-Wallis with Dunn's multiple comparison test. For identifying the relationships between the microbial community compositions and the environmental variables, principal component analysis (PCA) plots were visualized using the function fviz_pca_var from the R package (version 4.3.3) factoextra v1.0.7.

Results

Spatial dynamics of dissolved methane at the river delta:

In 2021, methane concentrations within the Rhône River a few km before it enters the lake were low (< 70 nM) throughout spring and summer (Table S3). Methane concentrations in the sublacustrine canyon and the lake delta were one or two orders of magnitudes greater (up to 3200 nM) than those measured in the river (Fig. 2), attesting that the deltaic region is a biogeochemical hotspot for methane production. Water column CH_4 concentrations were the greatest close to the shore or in the proximity of the river mouth (700-3200 nM, stations 1-7), and decreased towards offshore stations (8-15), outside of the sublacustrine canyon. In the sublittoral stations (1-7), methane concentrations were greater close to the sediment than those from the deepest and furthest stations (8-15). Interestingly, the observed metalimnetic methane concentrations (Fig. 2a) were two to three times higher than the hypolimnetic CH_4 (Fig. 2b) for the stations further from the deltaic regions (Station no. 10-13).

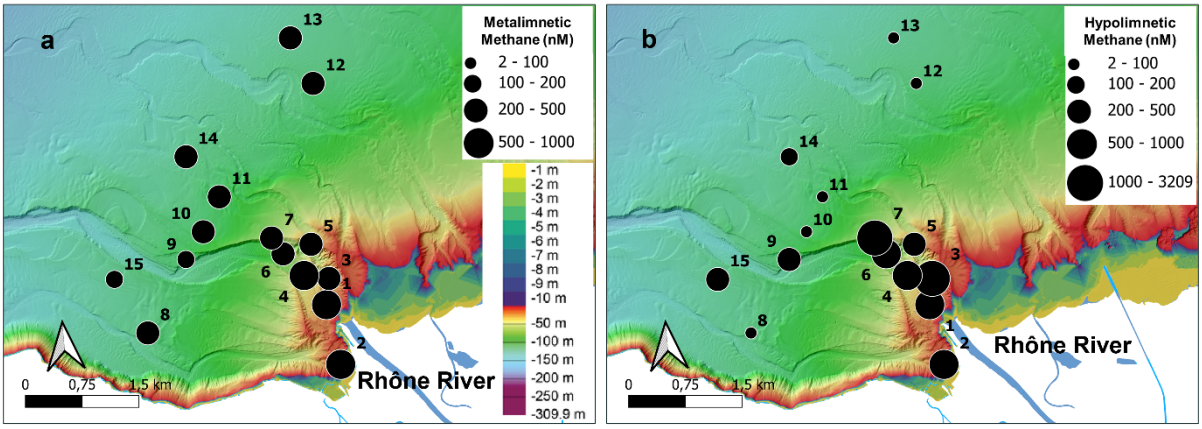

Fig. 2 Temporal variability of dissolved CH_4 concentration at the Rhône River delta. The size of the circles reflects the dissolved CH_4 concentrations (nM) at the metalimnion **(a)** and the hypolimnion **(b)** in the 15 sampling stations near the river delta in July 2021. The water

depth distribution (Metalimnion: 17-24 m, and Hypolimnion: 27- 172 m) can be found in Fig. 1. The active sublacustrine canyon for the Rhône River is visible from the bathymetry.

Temporal dynamics of metalimnetic methane at LéXPLORE:

The years 2021 and 2022 were characterized by drastically different meteorological conditions. The year 2022 was warmer than 2021, leading to lake surface temperatures being 4°C warmer in July, and a greater water column stability (Fig. 3 and S1). Pelagic methane in Lake Geneva varied seasonally and yearly, with lake surface temperature and strength of stratification. Methane supersaturation occurred as metalimnetic peaks for all dates when the lake was stratified, but one (5/7/21, when the maximum concentrations were above the thermocline). In the year 2021, methane concentrations measured at LéXPLORE increased from 50-69 nM (within the upper 15 m layer) in April to 242-372 nM (from 5-15 m) in July (Fig. 3, a-f). Methane concentrations were consistently highest in July over the years and decreased as stratification declined during the fall (in October). Similarly, turbidity peaks developed at the thermocline as stratification strengthened (Fig. 3, g-i and S1). While the signal attributed to the Rhône turbidity was weak in 2021, the metalimnetic turbidity peak was strong in July of 2022, consistent with a vertically well-constrained Rhône interflow across a more stable metalimnion (Fig. 3 and S2). Altogether, CH_4 concentrations at metalimnetic depths were positively and significantly correlated to the depth-specific N^2 stability (Fig. S1, $R^2 = 0.51$, $p < 10^{-6}$, $n = 30$). In 2021, the metalimnetic CH_4 concentration was not correlated to Chl *a* or turbidity whereas in 2022 it was correlated to turbidity (Table S4).

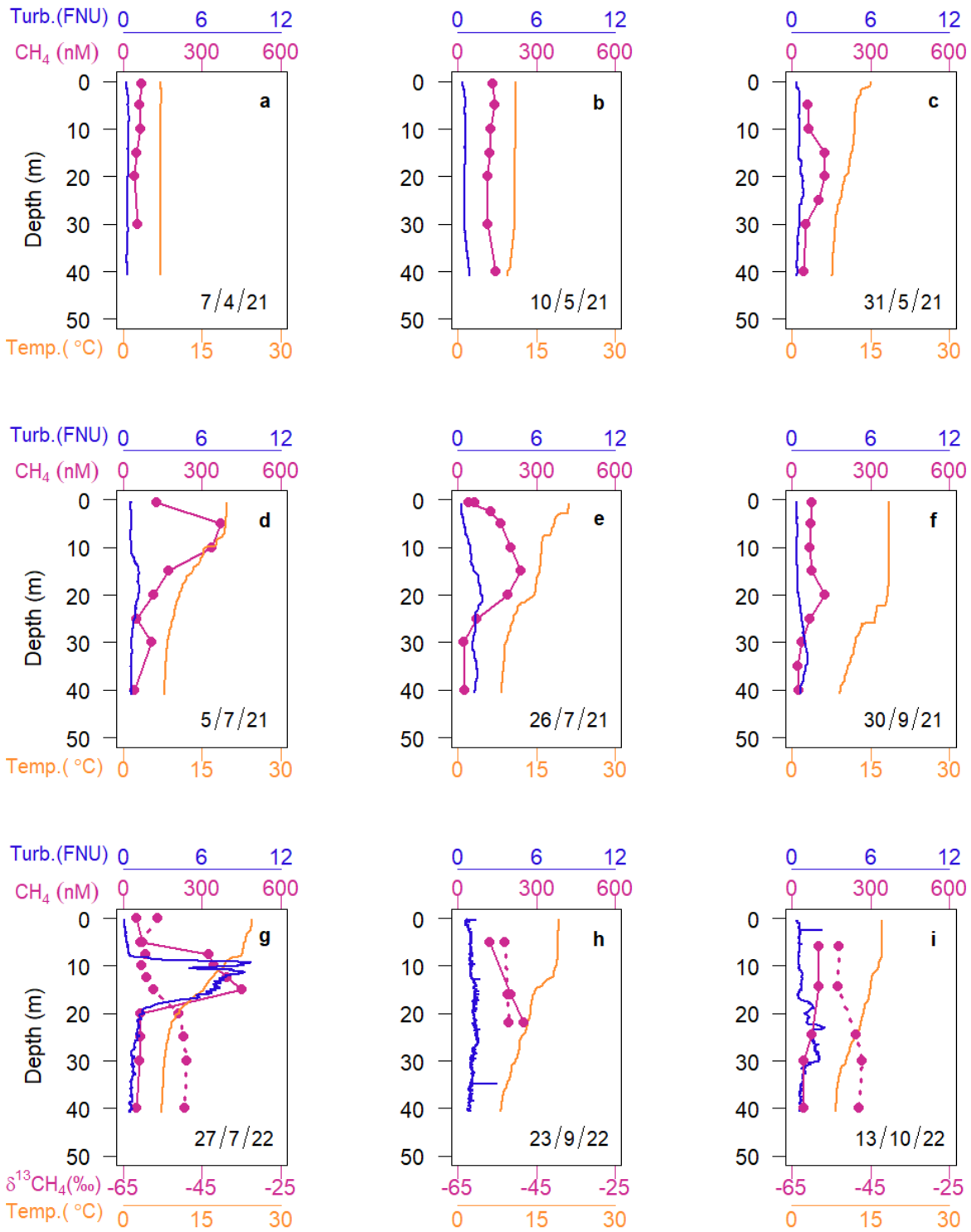

Fig. 3 Seasonal variability of vertical profiles of dissolved CH_4 concentration at the LéXPLORE station. CH_4, temperature (Temp.), and turbidity (Turb.) are shown respectively for 2021 **(a-f)** and for 2022 **(g-i)** and were measured using the multiparameter probe. The depth distributions of $\delta^{13}C$ CH_4 (‰) at the LéXPLORE station in 2022 **(g-i)** are represented as

dotted lines. Color codes for environmental parameters in both years are shown respectively in graphs **a, d,** and **g**.

The methane isotopic values ranged from −60.3‰ to −57.3‰, with the highest values within the metalimnetic peak (Fig. 3, g-i). Lower methane concentrations in the summer of July-October 2022 had higher isotopic values (r = -0.74, p =0.002, n =18), consistent with significant methane loss through oxidation (DelSontro et al. 2018).

Link with microbial community composition at LéXPLORE:

Targeted amplicon sequencing of different groups of planktonic bacteria for samples collected in July of 2022 revealed five predominant phyla: Proteobacteria (28-37%), Actinobacteriota (13-21%), Bacteroidota (22-36%), Cyanobacteria (0.5-11%), and Verrucomicrobiota (3-9%) (Fig. 4a). In September and October 2022, Actinobacteria and Cyanobacteria increased in relative abundance while they decreased in October (see Fig. S3 and S4). Phyla with potential for OMP, *i.e.*, Cyanobacteria, were the 3rd-4th most common bacterial taxa across all sampling depths and were most abundant in the upper layers throughout 2022 (Fig. S5). Although Cyanobacteria are expected to be the dominant contributors to OMP (Perez-Coronel and Michael Beman 2022), 95-97% of the copies of the *phnJ* gene detected belonged to the Proteobacteria phylum in July (Fig. 4b). No copies of the *mcrA* gene were detected (Fig. S6).

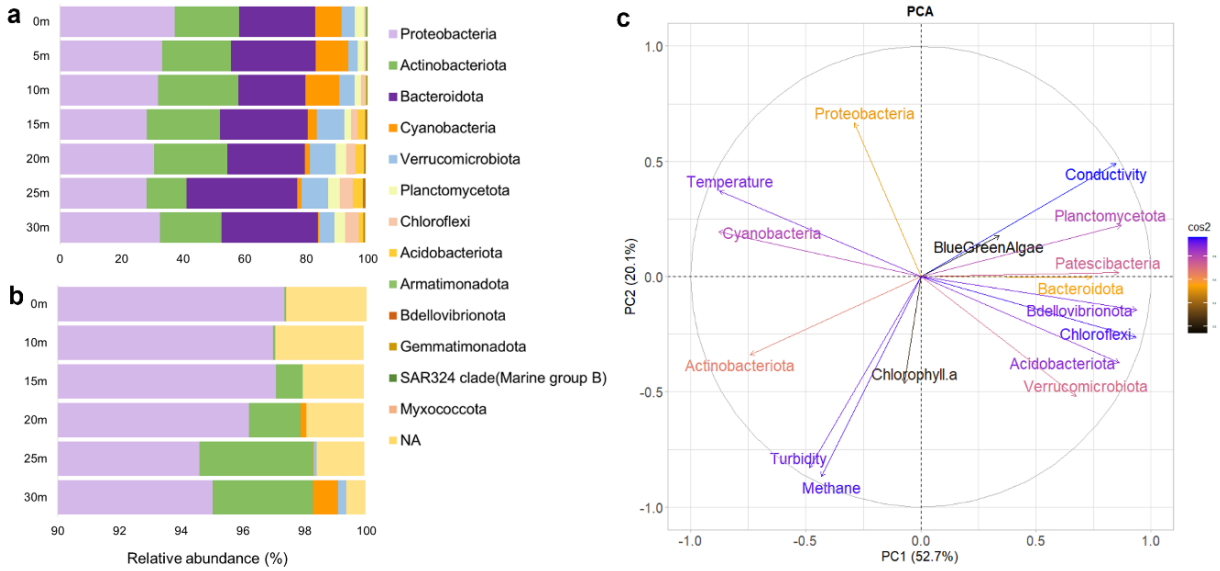

Fig. 4 Microbial community compositions and their relationship with environmental parameters at the LéXPLORE station. The relative abundance of bacterial phyla using the Universal bacteria primer **(a)** and the *phnJ* gene primer **(b)** respectively, were obtained from samples collected at 0-30 m depth in July 2022. **(c)** Principal Component Analysis (PCA) of bacterial phyla and biogeochemical data from vertical profile in July 2022 are projected on orthogonal axes with the two main dimensions (PC1 and PC2). Only significant environmental variables are represented and the color indicates the weight of the contribution. The higher values for each variable are positively scattered along the component's axis. Microbial community composition is obtained from the relative sequence abundance of bacterial phyla using the universal bacteria primer and the *phnJ* gene primer (Table S2).

PCA was used to identify the potential association of planktonic microorganisms such as Cyanobacteria with metalimnetic methane peak (Fig. 4c). About 52.7% of the variability was accounted for by the first principal component (PC1), and 20.1% by PC2. Temperature, Cyanobacteria relative abundance, and conductivity had the greatest weight on PC1. In fact, most of the planktonic variability was explained by the physical structure of the water column

in summer. CH_4 and turbidity had the greatest weight on PC2 and were orthogonal to most of the variables related to planktonic composition, including cyanobacteria relative abundance. Results did not point to any direct link between planktonic community composition and the metalimnetic methane peak. Dissolved CH_4 was more related to turbidity and the phylum Actinobacteriota than to Cyanobacteria.

Spatial distribution of the metalimnetic methane peak along the directional interflow:

For the spatial summer campaign of 2022, the distribution of dissolved CH_4 concentration in the metalimnion exhibited significant variability across sampling stations (Fig. 5a and S7). The metalimnetic methane peak was greatest at StaA (418-439 nM), 0.35 km away from the Rhône River delta, and then decreased three-fold towards further stations, up to StaD (103-169 nM, 6 km away from the Rhône delta). At LéXPLORE (staE, approximately 19 km away from the Rhône delta), there was a rebound of CH_4 concentrations (204-251 nM). The variability of CH_4 isotopic values at the metalimnion mirrors that of CH_4 concentrations (Fig. 5b), with the lightest isotopic composition at StaA (−59.8‰ to −60.2‰), and enrichment towards more distal stations (−51.3‰ to −52.1‰), consistent with methane loss through oxidation. Temperature within the metalimnion did not vary significantly across stations (Fig. 5c and S7). The metalimnetic turbidity was maximal closest to the Rhône delta (StaA), fading out towards StaD and StaE, so the CH_4 concentration across stations was positively correlated with turbidity ($r = 0.70$, $p < 10^{-4}$, Fig. 5d and 5e). Methane measured from surface sediment in the littoral zone of the Rhône delta and close to StaE in July 2023 exhibited light isotopic values typical for acetoclastic methanogenesis (−64.8‰ to −74.3‰ in the Rhône delta and −56.8‰ to −76.2‰ near the LéXPLORE station, Fig. 5f). The Keeling plot distribution (Fig. f) between metalimnetic CH_4 and its isotopic values (color points) revealed a negative

relationship with increasing distance from the river mouth whose intercept indicates a CH_4 source consistent with the isotopic composition measured in sediment samples.

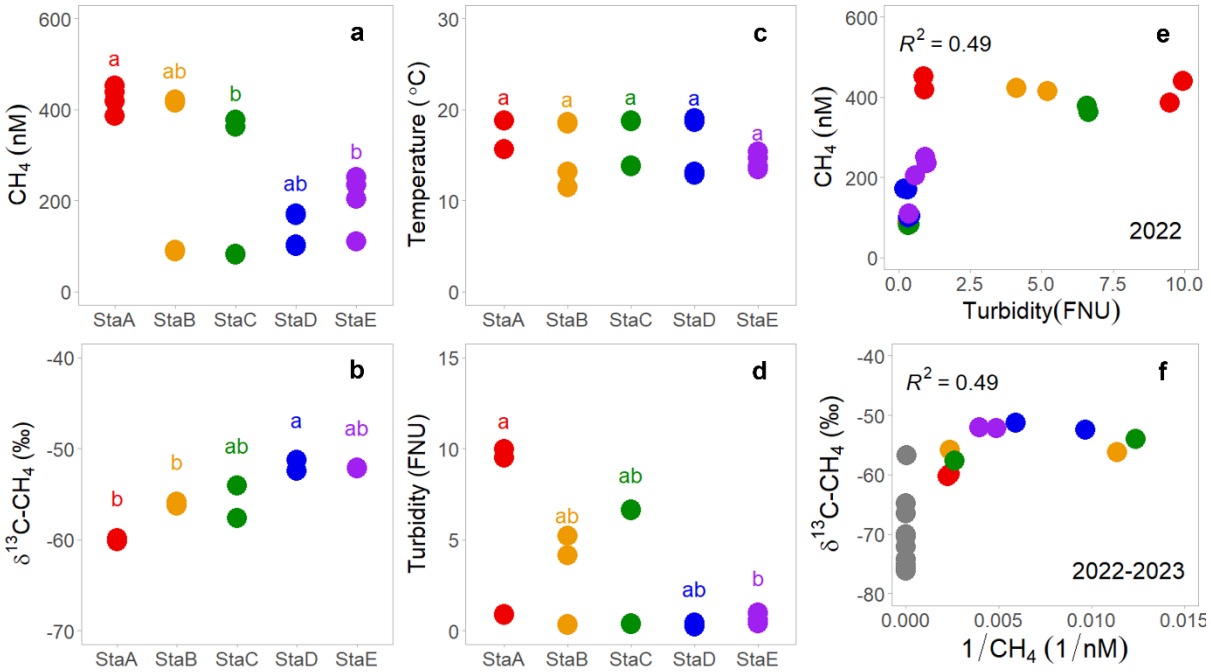

Fig. 5 Spatio-temporal patterns of biogeochemical properties in September 2022. (a-d) The plots show the value for the two depths (between 13-25 m, two replications per depth; see Fig. S7) in each sampling station where StaA was located in the Rhône River delta and StaE was the LéXPLORE station towards the lake center. Stations with the same letter (a,b) denote the variable at which performance measures are not significantly different, as indicated by Kruskal-Wallis with Dunn's multiple comparison test ($p < 0.05$, 95% confidence level). **(e)** The relationship of metalimnetic methane distribution with turbidity is shown here using linear regression analysis. Keeling plot **(f)** for the samples collected at the five stations in 2022 (colored dots) and sediment samples collected at the four stations in 2023 (silver dots). The colors of the dots correspond to the color code used for the sampling stations shown in **a-f**.

Sequencing data again revealed present and abundant cyanobacteria in the metalimnion (Fig. S4 and S5) at all different stations across the lake. The dominant microbial communities in September were Proteobacteria (22-43%), Actinobacteriota (18-39%), Cyanobacteria (5-45%), Bacteroidota (7-17%), and Verrucomicrobiota (2-7%). The population of Cyanobacteria increased in relative abundance from 4th place in the Rhône delta (StaA) to 3rd place at the StaB-StaE (Fig. S4). A prominent peak in abundance (45.5%) of Cyanobacteria was observed at the 15 m water depth of StaB, indicating it is the most abundant phylum at that station (Fig. S4 and S5). Nevertheless, PCA-based analysis revealed that CH_4, cyanobacteria, and turbidity have the greatest weight in PC1 and opposite signs (Fig. S4). In other words, there was a negative relationship between CH_4 and cyanobacteria in Lake Geneva. Instead, the microbial phyla Proteobacteria and Bacteroidota were most related to CH_4 in September (Fig. S4) which contrasts with the coupling of dissolved CH_4 and Actinobacteria in July (Fig. 4c).

Discussion

Up until now, a metalimnetic methane peak has only been measured sporadically in Lake Geneva (Donis et al. 2017). Our spatio-temporal survey of pelagic stations over the years 2021 and 2022 (Stations A-E, including LéXPLORE, Stations 9-15) confirms that the metalimnetic methane peak during lake stratification is a recurrent feature even for a lake of almost 600 km^2. We report maximum concentrations of *ca.* 400 nM for the metalimnetic methane peak (Fig. 3), which is of similar magnitude to that observed in smaller lakes, such as Lake Stechlin (Grossart et al. 2011) or Uberlingen, a deep basin of Lake Constance (Peeters et al. 2019), and small mountain lakes in Japan (Khatun et al. 2019, 2020; 200-600 nM). However, such concentrations are somewhat greater than had been previously measured in neighboring peri-alpine lakes (Switzerland, Lugano, 16-57 nM, Blees et al. 2015), or the large Lake Biwa (Murase et al. 2003, 2005; 150 nM). It should be noted that some of our pelagic (depth > 100 m) sampling stations (except StaD), were within 1 km distance from the lake shore and are not representative of the lake center. Proximity to the shore might be partly responsible for the metalimnetic methane peak concentrations being greater than what had been previously measured in comparable lakes.

Weak support for in situ production of the metalimnetic methane peak:

Over two consecutive years, metalimnetic methane peak development at LéXPLORE (*i.e.*, StaE) coincided with the stratification of the water column. Overall, the greatest dissolved CH_4 concentrations occurred at depths and dates of greatest water column stability (Fig. 3 and S1), as observed in other freshwater lakes (Murase et al. 2003; Bartosiewicz et al. 2023). The greater water column stability in 2022 can be attributed to warmer and considerably drier weather that year compared to 2021, resulting in twofold greater metalimnetic methane peaks.

The methane peak in July 2021 is an exception to the general pattern because it was observed in the epilimnion, at a depth of low water stability indicating the possibility of local production. However, no significant correlation between Chl *a* and metalimnetic CH_4 was observed in 2021 or 2022 (Table S4). Dissolved oxygen concentration was coupled with Chl *a* and turbidity peaks in summer 2022 (Fig. S2), but the presence of DO is not conclusive for OMP in the context of Lake Geneva because both the primary production and the interflow are sources of DO to the water column. The occurrence of OMP can also be interpreted using molecular tools (Fig. 4). For example, planktonic microbial communities such as cyanobacteria possessing the *phnJ* genes can cleave the C-P bond of methylphosphonates (MPn), and thereby produce methane aerobically (Blees et al. 2015; Yao et al. 2016; Khatun et al. 2019). The most probable mechanism of OMP is suspected to be the co-dependence of microbial communities synthesizing and cleaving MPn under nutrient-limited conditions (Bižić-Ionescu et al. 2018). However, molecular data from 2022 provide little support for OMP in the metalimnion of Lake Geneva. Cyanobacteria were present in the upper water column in 2022 (Fig. S5) but we found no significant relationship (r = -0.45, p <0.05) between their vertical distribution and dissolved methane concentration. Actinobacteriota can indirectly impact metalimnetic methane peak formation as they possess the *phnJ* genes (Yu et al. 2013; Ju et al. 2015; Wang et al. 2021) and commonly synthesize phosphonate (a substrate for oxic methanogenesis) but the relative abundance of *phnJ* genes affiliated with Actinobacteriota was <1% in the metalimnion (Fig. 4b). Proteobacteria, which predominate throughout the water column, exhibited no relationship with CH_4 although Proteobacteria are often associated with MPn-driven CH_4 production in both marine and freshwater ecosystems (Carini et al. 2014; Wang et al. 2017; Sosa et al. 2019). Overall, since no relationships between relative *phnJ* gene abundance and metalimnetic CH_4 concentration were observed, phosphonate metabolism is unlikely to be the underlying cause of metalimnetic methane peak

in Lake Geneva. Our results indicate that even if microbial CH_4 production contributes to metalimnetic methane peaks in Lake Geneva, there must exist other driving mechanisms.

High support for the transport of ex situ-produced methane through the interflow:

While methane concentrations were low within the Rhône River itself (70 nM, Table S3), the CH_4 concentrations reached high values in the river delta (>2,000 nM, Fig.1). The Rhône River delta is a continuous depositional zone for riverine and littoral organic matter that has been previously identified as a hotspot of potential CH_4 production and emission (Sollberger et al. 2014; Corella et al. 2016). These earlier studies revealed high methane production at the sublittoral depths of 20-50 m in the Rhône delta canyons (Sollberger et al. 2014). Sediment gas samples from the sublittoral Rhône delta confirmed the production of methane, whose isotope composition (Fig. 5f, −66.5‰ to −76.2‰) is typical for acetoclastic methanogenesis (Whiticar and Faber 1986; Conrad 2009). Within the river mouth, at sublittoral stations, where the water column is weakly stratified, methane concentrations were high in both the hypolimnion and metalimnion (Stations 1-7), consistent with methane production in sublittoral habitats. At further pelagic stations (Station 9-15 but also Stations A-D), methane reached peak concentrations in the metalimnion only, ruling out significant methane production from deep pelagic sediments. From our Keeling plots (Fig. 5f) we can infer significant oxidation during transport and extrapolate a methane source with a depleted $\delta^{13}C$ methane value (−51.3‰ to −60.2‰), consistent with acetoclastic methanogenesis (Angel et al. 2011) and similar to the $\delta^{13}C$- CH_4 measured in deltaic sediments (−56‰ to −76.2‰).

Transport of deltaic methane through the interflow:

Turbidity was the main factor consistently correlated with methane concentrations across dates, stations, and years, especially in 2022. Because the Rhône is a glacier-fed river, the sediment-laden turbidity, mostly consisting of mineral particles (Escoffier et al. 2022) has been long established as a tracer of the interflow and intrusion within the lake (Ishiguro and Okubo 2006; Hasegawa-Ishiguro and Okubo 2008; Dominik et al. 1983). While the larger particles are deposited close to the river mouth, lighter particles can be conveyed several km away in the Northern branch of the interflow (Escoffier et al. 2022), even if the turbidity signal fades due to particle deposition and dispersion (Fig. 5d). Seasonal tracing using water isotopes have confirmed that stratification vertically constrains the dispersion of the Rhône interflow in the metalimnion (Cotte and Vennemann 2020). In other words, when local stability increases, the interflow is more concentrated and vertically constrained thus traveling greater distances within the lake metalimnion. Indeed, our vertical profiling of the water column reveals that methane concentration is greater where and when both the stability and turbidity are maximal, consistent with the idea that a more defined and less diluted interflow favors methane transport from distant production sites (Fig. 1 and Fig. 6). Similarly, when stratification begins to weaken, metalimnetic methane concentrations and turbidity fade with distance from the river mouth due to dispersion (Fig. 5 and 6).

As methane is transported across the lake and encounters oxygen, it is expected that oxidation leaves behind isotopically heavier methane as demonstrated in Lake Biwa (Tsunogai et al. 2020). Indeed, the negative correlation between the metalimnetic methane concentration and its isotope composition is consistent with methane loss due to oxidation during long-range transport (Fig. 5f). Proteobacteria are known to oxidize CH_4 aerobically (Wang et al. 2021; Martin et al. 2021), but the presence of oxic methanotrophs remains unknown as the *pmoA* gene was not targeted here. A back-of-the-envelope estimate of methane loss per day can be performed using the dissolved CH_4 flux between stations and the following assumptions: (*i*) a

constant water velocity of 0.01 ms^{-1} represents a realistic mean value for water flow under calm conditions in the thermocline (Fig. 1), (*ii*) the water was followed a straight path between the different stations, meaning the estimated travel time is the minimum travel time, and (*iii*) it confined methane transport within the interflow with limited diffusive loss. Under such assumptions based on Fig. 5, at the depth of interflow, an oxidation rate of 0-37 nMd^{-1} could explain the methane loss between the two stations. These calculated CH_4 oxidation rates are similar to measured volumetric CH_4 oxidation rates of 22-26 nMd^{-1} reported in other lakes (Günthel et al. 2019; Langenegger et al. 2022), thereby indicating limited methane oxidation within the interflow.

Other possible sources for metalimnetic methane at the LéXPLORE station:

Overall, our results suggest that the directional and efficient transport of sublittoral (deltaic) methane through the interflow is the dominant mechanism for the metalimnetic peak in the pelagic zone of Lake Geneva. The more intensive spatial survey, however, suggests potential multiple origins for pelagic methane throughout the year at the LéXPLORE station. In July 2021, the peaks of methane, some of which occurred even in the epilimnion, did not match with the turbidity peaks, suggesting the Rhône interflow might not be the only process for pelagic methane. Unfortunately, molecular sequencing and isotopic data for 2021 are lacking, so we cannot assess whether OMP in the upper layers of the lakes contributed to the methane peak at this specific date. In addition, the longitudinal sampling along the North-Eastern branch of the gyre in September 2022 showed a significant rebound of methane at the metalimnion between Station D (StaD) and LéXPLORE (StaE), pointing to an additional methane source. Additionally, the isotopic composition in the metalimnetic peak in the late summer sampling was significantly heavier than the one observed at the maximum of the stratification (July 2022), when the interflow transport was maximal. Sediment sampling in

between the lake shore and the LéXPLORE station revealed significant methane concentrations in the sublittoral sediment, with a distinctive $\delta^{13}C$- CH_4 of −56‰ (*i.e.* heavier than in the deltaic methane, Fig. 5f). Altogether, data indicate that not all methane at LéXPLORE might be coming from the deltaic region, and some may originate from a sublittoral source at a shorter range (closest shore). When the lake is weakly stratified and interflow transport loses momentum, methane produced in the sublittoral sediment close to LéXPLORE might also diffuse and contribute to the pelagic methane (Fig. 6), both in the metalimnetic and surface mixed layers.

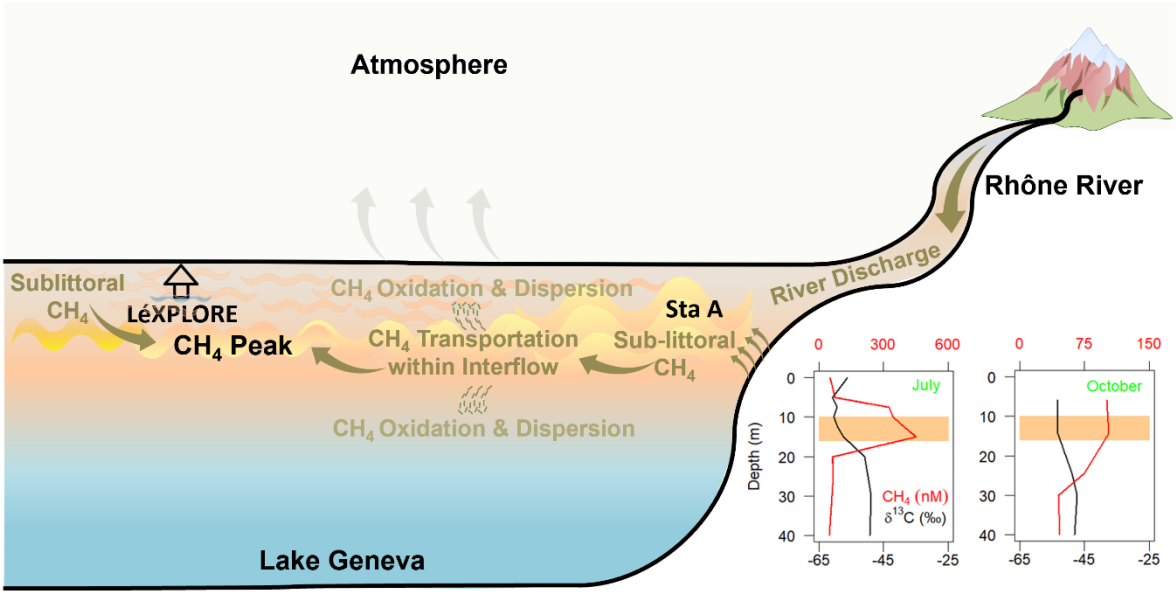

Fig. 6 Schematic diagram of the formation of the metalimnetic methane peak in the stratified water column of Lake Geneva. Methane accumulation in the metalimnion may be caused by transport of sublittoral methane via the Rhône River inflow from StaA (near the river mouth) towards StaE (LéXPLORE station). The solid arrows indicate the movement of water parcels/dissolved matter. There is a shift in CH_4 concentration and $\delta^{13}C$ CH_4 values in the upper 40m depth at the LéXPLORE station with the seasonal weakening of stratification (Lower right panel).

Conclusions

Our present study demonstrates that long-range transport of sublittoral-produced methane leading to metalimnetic methane accumulation is also possible in a large and deep lake like Lake Geneva (Fig. 6), thus revising our conception of volatile gas transport across standing water bodies. It can be implied that the tributary river discharge during the summer season may induce internal waves and play a crucial role in stirring up sediments, promoting mixing, and influencing the release of dissolved methane from the deltaic hypolimnion to the metalimnion. Even if these biogeochemical hotspots for methane production represent only a very limited fraction of the surface area of large and deep lakes, the efficiency of the lateral transport within a well-constrained metalimnion due to turbulent diffusion, internal waves, and advection, can expand the dispersion of sublittorally produced methane to > 20 km away from the production area. Elucidating the directional transportation pathways of deltaic methane from the Rhone River delta toward the lake center is the next critical step to deepen our understanding of how the riverine and the in-lake processes interact in transporting sublittoral methane to form metalimnetic methane peaks in large lakes.

Acknowledgments

SK was funded by an excellence post-doctoral fellowship from the Dean of the Faculty of Geoscience and Environment, University of Lausanne (UniL). We are grateful to the entire LéXPLORE consortium for supporting us in conducting our study, especially the five involved partner institutions: University of Lausanne, EPFL, Eawag, University of Geneva, and INRAE-USMB (CARRTEL). We thank Lavanchy Sébastien Manuel, Cunillera Guillaume Gilbert René, Jeremy Keller, Floreana Marie Miesen, Aurélien Ballu and, and fieldwork participant: Emma Bonvin, for helping us in organizing the field campaigns. We are indebted to Laetitia Monbaron, Micaela Faria, Serge Robert, and Patrick Kathriner, for helping to conduct the laboratory analyses. We are grateful to all the laboratory members of the University of Lausanne and the EAWAG in Kastanienbaum for their consistent support.

References

Ahlfeld, D., A. Joaquin, J. Tobiason, and D. Mas. 2003. Case Study: Impact of Reservoir Stratification on Interflow Travel Time. J. Hydraul. Eng. **129**: 966–975. doi:10.1061/(ASCE)0733-9429(2003)129:12(966)

Angel, R., D. Matthies, and R. Conrad. 2011. Activation of Methanogenesis in Arid Biological Soil Crusts Despite the Presence of Oxygen J.A. Gilbert [ed.]. PLoS ONE **6**: e20453. doi:10.1371/journal.pone.0020453

Baracchini, T., A.Wüest, and D. Bouffard. 2020. Meteolakes: An operational online three-dimensional forecasting platform for lake hydrodynamics. Water Res. **172**: 115529. doi:10.1016/j.watres.2020.115529

Bartosiewicz, M., J. Venetz, S. Läubli, O. Sepúlveda Steiner, D. Bouffard, J. Zopfi, and M-F. Lehmann. 2023. Detritus-hosted methanogenesis sustains the methane paradox in an alpine lake. Limnol. Oceanogr. **68**: 248-264. doi:org/10.1002/lno.12263

Bastviken, D., J. Cole, M. Pace, and L. Tranvik. 2004. Methane emissions from lakes: Dependence of lake characteristics, two regional assessments, and a global estimate. Glob. Biogeochem. Cycles **18**: 2004GB002238. doi:10.1029/2004GB002238

Bižić, M., T. Klintzsch, D. Ionescu, and others. 2020. Aquatic and terrestrial cyanobacteria produce methane. Sci. Adv. **6**: eaax5343. doi:10.1126/sciadv.aax5343

Bižić-Ionescu, M., D. Ionescu, M. Günthel, K. W. Tang, and H.-P. Grossart. 2018. Oxic Methane Cycling: New Evidence for Methane Formation in Oxic Lake Water, p. 1–22. *In* A.J.M. Stams and D. Sousa [eds.], Biogenesis of Hydrocarbons. Springer International Publishing.

Blees, J., H. Niemann, M. Erne, J. Zopfi, C. J. Schubert, and M. F. Lehmann. 2015. Spatial variations in surface water methane super-saturation and emission in Lake Lugano, southern Switzerland. Aquat. Sci. **77**: 535–545. doi:10.1007/s00027-015-0401-z

Bouffard, D., and U. Lemmin. 2013. Kelvin waves in Lake Geneva. J. Gt. Lakes Res. **39**: 637–645. doi:10.1016/j.jglr.2013.09.005

Callahan, B. J., P. J. McMurdie, M. J. Rosen, A. W. Han, A. J. A. Johnson, and S. P. Holmes. 2016. DADA2: High-resolution sample inference from Illumina amplicon data. Nat. Methods **13**: 581–583. doi:10.1038/nmeth.3869

Carini, P., A. E. White, E. O. Campbell, and S. J. Giovannoni. 2014. Methane production by phosphate-starved SAR11 chemoheterotrophic marine bacteria. Nat. Commun. **5**: 4346. doi:10.1038/ncomms5346

Cimatoribus, A. A., U. Lemmin, and D. A. Barry. 2019. Tracking Lagrangian transport in Lake Geneva: A 3D numerical modeling investigation. Limnol. Oceanogr. **64**: 1252–1269. doi:10.1002/lno.11111

CIPEL. 2019. Conseil scientifque de la commission internationale pour la protection des eaux du Léman contre la pollution. Rapports sur les études et recherches entreprises dans le bassin lémanique. Campagne 2018.

Conrad, R. 2009. The global methane cycle: recent advances in understanding the microbial processes involved. Environ. Microbiol. Rep. **1**: 285–292. doi:10.1111/j.1758-2229.2009.00038.x

Conrad, R., M. Klose, and A. Enrich-Prast. 2020. Acetate turnover and methanogenic pathways in Amazonian lake sediments. Biogeosciences **17**: 1063–1069. doi:10.5194/bg-17-1063-2020

Corella, J. P., J.-L. Loizeau, K. Kremer, and others. 2016. The role of mass-transport deposits and turbidites in shaping modern lacustrine deepwater channels. Mar. Petrol. Geol. **77**: 515–525. doi:10.1016/j.marpetgeo.2016.07.004

Cotte, G., and T. W. Vennemann. 2020. Mixing of Rhône River water in Lake Geneva: Seasonal tracing using stable isotope composition of water. J. Gt. Lakes Res. **46**: 839–849. doi:10.1016/j.jglr.2020.05.015

DelSontro, T., P. A. Del Giorgio, and Y. T. Prairie. 2018. No Longer a Paradox: The Interaction Between Physical Transport and Biological Processes Explains the Spatial Distribution of Surface Water Methane Within and Across Lakes. Ecosystems **21**: 1073–1087. doi:10.1007/s10021-017-0205-1

Dominik, J., Burrus, D., and J-P. Vernet. 1983. A preliminary investigation of the Rhone River plume in eastern Lake Geneva. J. Sediment. Res. **53**: 159-163. doi :org/10.1306/212F817A-2B24-11D7-8648000102C1865D

Donis, D., S. Flury, A. Stöckli, J. E. Spangenberg, D. Vachon, and D. F. McGinnis. 2017. Full-scale evaluation of methane production under oxic conditions in a mesotrophic lake. Nat. Commun. **8**: 1661. doi:10.1038/s41467-017-01648-4

Encinas Fernández, J., F. Peeters, and H. Hofmann. 2016. On the methane paradox: Transport from shallow water zones rather than in situ methanogenesis is the major source of CH_4 in the open surface water of lakes. JGR Biogeosciences **121**: 2717–2726. doi:10.1002/2016JG003586

Escoffier, N., P. Perolo, T. Lambert, J. Rüegg, D. Odermatt, T. Adatte, T. Vennemann, and M-E. Perga. 2022. Whiting events in a large peri-alpine lake: Evidence of a catchment-scale process. J. Geophy. Res.: Biogeosci. **127**: e2022JG006823. doi:org/10.1029/2022JG006823

Ernst, L., B. Steinfeld, U. Barayeu, and others. 2022. Methane formation driven by reactive oxygen species across all living organisms. Nature **603**: 482–487. doi:10.1038/s41586-022-04511-9

Fofonoff, N. P., and R. C. Millard Jr. 1983. Algorithms for the computation of fundamental properties of seawater. Endorsed by Unesco/SCOR/ICES/IAPSO Joint Panel on Oceanographic Tables and Standards and SCOR Working Group 51.

Giovanoli, F., and A. Lambert. 1985. The stratification of the Rhône in Lake Geneva: results of current measurements in August 1983. Swiss J. Hydrol. **47**: 159-178.

Giovanoli, F. 1990. Horizontal transport and sedimentation by interflows and turbidity currents in Lake Geneva. In Large lakes: Ecological structure and function. Springer Berlin Heidelberg: 175-195. doi:org/10.1007/978-3-642-84077-7_9

Grossart, H.-P., K. Frindte, C. Dziallas, W. Eckert, and K. W. Tang. 2011. Microbial methane production in oxygenated water column of an oligotrophic lake. Proc. Natl. Acad. Sci. U.S.A. **108**: 19657–19661. doi:10.1073/pnas.1110716108

Günthel, M., D. Donis, G. Kirillin, D. Ionescu, M. Bizic, D. F. McGinnis, H.-P. Grossart, and K. W. Tang. 2019. Contribution of oxic methane production to surface methane emission in lakes and its global importance. Nat. Commun. **10**: 5497. doi:10.1038/s41467-019-13320-0

Halder, J., L. Decrouy, and T. W. Vennemann. 2013. Mixing of Rhône River water in Lake Geneva (Switzerland–France) inferred from stable hydrogen and oxygen isotope profiles. J. Hydrol. **477**: 152–164. doi:10.1016/j.jhydrol.2012.11.026

Hasegawa-Ishiguro, N., and K. Okubo. 2008. Glacial melt inflows into Lake Geneva. SIL Proceedings, 1922-2010 **30**: 643–646. doi:10.1080/03680770.2008.11902207

Hilt, S., H. Grossart, D. F. McGinnis, and F. Keppler. 2022. Potential role of submerged macrophytes for oxic methane production in aquatic ecosystems. Limnol. Oceanogr. **67**. doi:10.1002/lno.12095

IPCC. 2021. Chapter 5: Global Carbon and other Biogeochemical Cycles and Feedbacks. In Climate Change 2021: The Physical Science Basis. Contribution of Working Group I to the Sixth Assessment Report of the Intergovernmental Panel on Climate Change. Cambridge University Press: 673–816. doi:10.1017/9781009157896.007

Ishiguro, N., and G. Balvay. 2003. L'écoulement des eaux du Rhône dans le lac Léman. Arch. Sci. **56**: 117–126. doi: 10.5169/seals-740434

Ishiguro, N., and K. Okubo. 2006. Double-diffusive convection in the thermocline of Lake Geneva. SIL Proceedings, 1922-2010 **29**: 1833–1836. doi:10.1080/03680770.2006.11903006

Ju, K.-S., J. Gao, J. R. Doroghazi, and others. 2015. Discovery of phosphonic acid natural products by mining the genomes of 10,000 actinomycetes. Proc. Natl. Acad. Sci. U.S.A. **112**: 12175–12180. doi:10.1073/pnas.1500873112

Kang, M., L. Liu, and H.-P. Grossart. 2024. Spatio-temporal variations of methane fluxes in sediments of a deep stratified temperate lake. iScience **27**: 109520. doi:10.1016/j.isci.2024.109520

Khatun, S., T. Iwata, H. Kojima, and others. 2019. Aerobic methane production by planktonic microbes in lakes. Sci. Total Env. **696**: 133916. doi:10.1016/j.scitotenv.2019.133916

Khatun, S., T. Iwata, H. Kojima, and others. 2020. Linking Stoichiometric Organic Carbon–Nitrogen Relationships to planktonic Cyanobacteria and Subsurface Methane Maximum in Deep Freshwater Lakes. Water **12**: 402. doi:10.3390/w12020402

Langenegger, T., D. Vachon, D. Donis, and D. F. McGinnis. 2022. Methane oxidation dynamics in a stratified lake: Insights revealed from a mass balance and carbon stable isotopes. Limnol. Oceanogr. **67**: 2157–2173. doi:10.1002/lno.12195

Li, M., C. Peng, Q. Zhu, X. Zhou, G. Yang, X. Song, and K. Zhang. 2020. The significant contribution of lake depth in regulating global lake diffusive methane emissions. Water Res. **172**: 115465. doi:10.1016/j.watres.2020.115465

Martin, G., A. J. Rissanen, S. L. Garcia, M. Mehrshad, M. Buck, and S. Peura. 2021. Candidatus Methylumidiphilus Drives Peaks in Methanotrophic Relative Abundance in Stratified Lakes and Ponds Across Northern Landscapes. Front. Microbiol. **12**: 669937. doi:10.3389/fmicb.2021.669937

Michalski, J., and U. Lemmin. 1995. Dynamics of vertical mixing in the hypolimnion of a deep lake: Lake Geneva. Limnol. Oceanogr. **40**: 809–816. doi:10.4319/lo.1995.40.4.0809

Michmerhuizen, C. M., R. G. Striegl, and M. E. McDonald 1996. Potential methane emission from north-temperate lakes following ice melt. Limnol. Oceanogr. **41**: 985-991. doi.org/10.4319/lo.1996.41.5.0985

Murase, J., Y. Sakai, A. Kametani, and A. Sugimoto. 2005. Dynamics of methane in mesotrophic Lake Biwa, Japan. Ecol. Res. **20**: 377–385. doi:10.1007/s11284-005-0053-x

Murase, J., Y. Sakai, A. Sugimoto, K. Okubo, and M. Sakamoto. 2003. Sources of dissolved methane in Lake Biwa. Limnology **4**: 91–99. doi:10.1007/s10201-003-0095-0

Nouchi, V., T. Kutser, A. Wüest, B. Müller, D. Odermatt, T. Baracchini, and D. Bouffard. 2019. Resolving biogeochemical processes in lakes using remote sensing. Aquat. Sci. **81**: 27. doi:10.1007/s00027-019-0626-3

Peeters, F., J. Encinas Fernandez, and H. Hofmann. 2019. Sediment fluxes rather than oxic methanogenesis explain diffusive CH_4 emissions from lakes and reservoirs. Sci. Rep. **9**: 243. doi:10.1038/s41598-018-36530-w

Peeters, F., and H. Hofmann. 2021. Oxic methanogenesis is only a minor source of lake-wide diffusive CH4 emissions from lakes. Nat. Commun. **12**: 1206. doi:10.1038/s41467-021-21215-2

Perez-Coronel, E., and J. Michael Beman. 2022. Multiple sources of aerobic methane production in aquatic ecosystems include bacterial photosynthesis. Nat. Commun. **13**: 6454. doi:10.1038/s41467-022-34105-y

Piton, V., F. Soulignac, U. Lemmin, B. Graf, H. K. Wynn, K. Blanckaert, and D. A. Barry. 2022. Tracing Unconfined Nearfield Spreading of a River Plume Interflow in a Large Lake

(Lake Geneva): Hydrodynamics, Suspended Particulate Matter, and Associated Fluxes. Front. Water **4**: 943242. doi:10.3389/frwa.2022.943242

Quast, C., E. Pruesse, P. Yilmaz, J. Gerken, T. Schweer, P. Yarza, J. Peplies, and F. O. Glöckner. 2012. The SILVA ribosomal RNA gene database project: improved data processing and web-based tools. NAR **41**: D590–D596. doi:10.1093/nar/gks1219

Riera, J. L., J. E. Schindler, and T. K. Kratz 1999. Seasonal dynamics of carbon dioxide and methane in two clear-water lakes and two bog lakes in northern Wisconsin, USA. Can. J. Fish. Aquat. Sci **56**: 265-274. doi.org/10.1139/f98-182

Rosentreter, J. A., A. V. Borges, B. R. Deemer, and others. 2021. Half of global methane emissions come from highly variable aquatic ecosystem sources. Nat. Geosci. **14**: 225–230. doi:10.1038/s41561-021-00715-2

Rudd, J. W. M., and R. D. Hamilton. 1978. Methane cycling in a eutrophic shield lake and its effects on whole lake metabolism 1. Limnol. Oceanogr. **23**: 337–348. doi:10.4319/lo.1978.23.2.0337

Saunois, M., R. B. Jackson, P. Bousquet, B. Poulter, and J. G. Canadell. 2016. The growing role of methane in anthropogenic climate change. Environ. Res. Lett. **11**: 120207. doi:10.1088/1748-9326/11/12/120207

Schroll, M., L. Liu, T. Einzmann, F. Keppler, and H.-P. Grossart. 2023. Methane accumulation and its potential precursor compounds in the oxic surface water layer of two contrasting stratified lakes. Sci. Total Env. **903**: 166205. doi:10.1016/j.scitotenv.2023.166205

Sobek, S., E. Durisch-Kaiser, R. Zurbrügg, N. Wongfun, M. Wessels, N. Pasche, and B. Wehrli. 2009. Organic carbon burial efficiency in lake sediments controlled by oxygen exposure time and sediment source. Limnol. Oceanogr. **54**: 2243–2254. doi:10.4319/lo.2009.54.6.2243

Sollberger, S., J. P. Corella, S. Girardclos, M.-E. Randlett, C. J. Schubert, D. B. Senn, B. Wehrli, and T. DelSontro. 2014. Spatial heterogeneity of benthic methane dynamics in the subaquatic canyons of the Rhone River Delta (Lake Geneva). Aquat. Sci. **76**: 89–101. doi:10.1007/s00027-013-0319-2

Sosa, O. A., D.J. Repeta, E. F. DeLong, M. D. Ashkezari, and D-M. Karl. 2019. Phosphate-limited ocean regions select for bacterial populations enriched in the carbon–phosphorus lyase

pathway for phosphonate degradation. Environ. Microbiol. **21**: 2402-2414. doi:org/10.1111/1462-2920.14628

Stevens, C. L., P. F. Hamblin, G. A. Lawrence, and F. M. Boyce. 1995. River-Induced Transport in Kootenay Lake. J. Environ. Eng. **121**: 830–837. doi:10.1061/(ASCE)0733-9372(1995)121:11(830)

Talling, J. F., and D. Driver. 1963. Some problems in the estimation of chlorophyll-a in phytoplankton. Proceedings of a conference on primary productivity measurements. U.S. atomic energy communication TID-7633:142–146.

Tang, K. W., D. F. McGinnis, D. Ionescu, and H.-P. Grossart. 2016. Methane Production in Oxic Lake Waters Potentially Increases Aquatic Methane Flux to Air. Environ. Sci. Technol. Lett. **3**: 227–233. doi:10.1021/acs.estlett.6b00150

Tsunogai, U., Y. Miyoshi, T. Matsushita, D. D. Komatsu, M. Ito, C. Sukigara, F. Nakagawa, and M. Maruo. 2020. Dual stable isotope characterization of excess methane in oxic waters of a mesotrophic lake. Limnol. Oceanogr. **65**: 2937–2952. doi:10.1002/lno.11566

Wang, Q., A. Alowaifeer, P. Kerner, and others. 2021. Aerobic bacterial methane synthesis. Proc. Natl. Acad. Sci. U.S.A. **118**: e2019229118. doi:10.1073/pnas.2019229118

Wang, Q., J. E. Dore, and T. R. McDermott. 2017. Methylphosphonate metabolism by *Pseudomonas* sp. populations contributes to the methane oversaturation paradox in an oxic freshwater lake. Environ. Microbiol. **19**: 2366–2378. doi:10.1111/1462-2920.13747

Whiticar, M. J., and E. Faber. 1986. Methane oxidation in sediment and water column environments—Isotope evidence. Org. Geochem. **10**: 759–768. doi:10.1016/S0146-6380(86)80013-4

Wüest, A., D. Bouffard, J. Guillard, B. W. Ibelings, S. Lavanchy, M. Perga, and N. Pasche. 2021. LÉXPLORE : A floating laboratory on Lake Geneva offering unique lake research opportunities. WIREs Water **8**: e1544. doi:10.1002/wat2.1544

Yao, M., C. Henny, and J. A. Maresca. 2016. Freshwater Bacteria Release Methane as a By-Product of Phosphorus Acquisition J.E. Kostka [ed.]. Appl. Environ. Microbiol. **82**: 6994–7003. doi:10.1128/AEM.02399-16

Yu, X., J. R. Doroghazi, S. C. Janga, J. K. Zhang, B. Circello, B. M. Griffin, D. P. Labeda, and W. W. Metcalf. 2013. Diversity and abundance of phosphonate biosynthetic genes in nature. Proc. Natl. Acad. Sci. U.S.A. **110**: 20759–20764. doi:10.1073/pnas.1315107110

Zimmermann, M., M. J. Mayr, H. Bürgmann, W. Eugster, T. Steinsberger, B. Wehrli, A. Brand, and D. Bouffard. 2021. Microbial methane oxidation efficiency and robustness during lake overturn. Limnol. Oceanogr. Letters **6**: 320–328. doi:10.1002/lol2.10209

Author Contributions

S.K., D.J., M.M, J.S.B., N.E., and M.E.P. performed the field survey. S.K. conducted the laboratory and gene sequence analyses. D.B. and C.J.S. supported in the data analyses and presentation. S.K. wrote the manuscript with the assistance of M.E.P. and J.S.B. All authors have read and agreed to the published version of the manuscript.

Data availability

Raw sequence files are available on the Sequence Read Archive of the National Center for Biotechnology (NCBI) under the bioproject accession number PRJNA1048867. Other relevant data included in this manuscript will be made available on the Swiss database.

Conflict of Interest

The authors declare no competing interests.

Long-range transport of littoral methane explains the metalimnetic methane peak in a large lake

Supplementary Information:

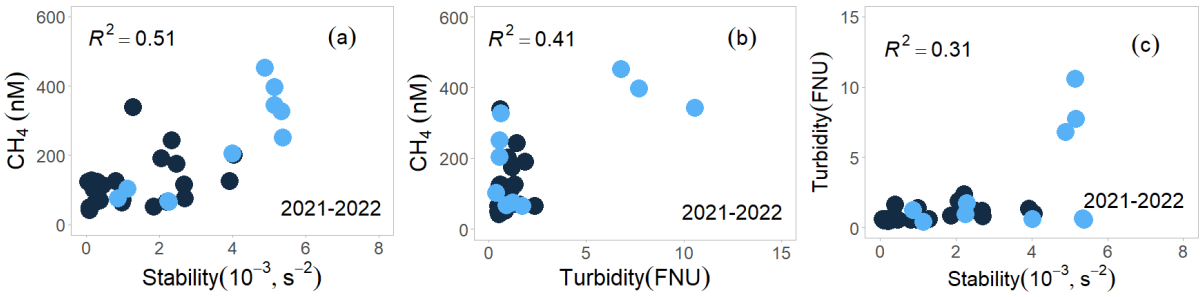

Fig. S1 Metalimnetic CH_4 relationships with stability and turbidity. The relationship of metalimnetic dissolved CH_4 concentration (nM) at the LéXPLORE station with N^2 stability **(a)** and turbidity **(b)**. **(c)** The relationship of turbidity and stability for the water samples collected from the metalimnion at the LéXPLORE station in 2021 and 2022. The black and blue circles respectively indicate the data obtained in 2021 and 2022.

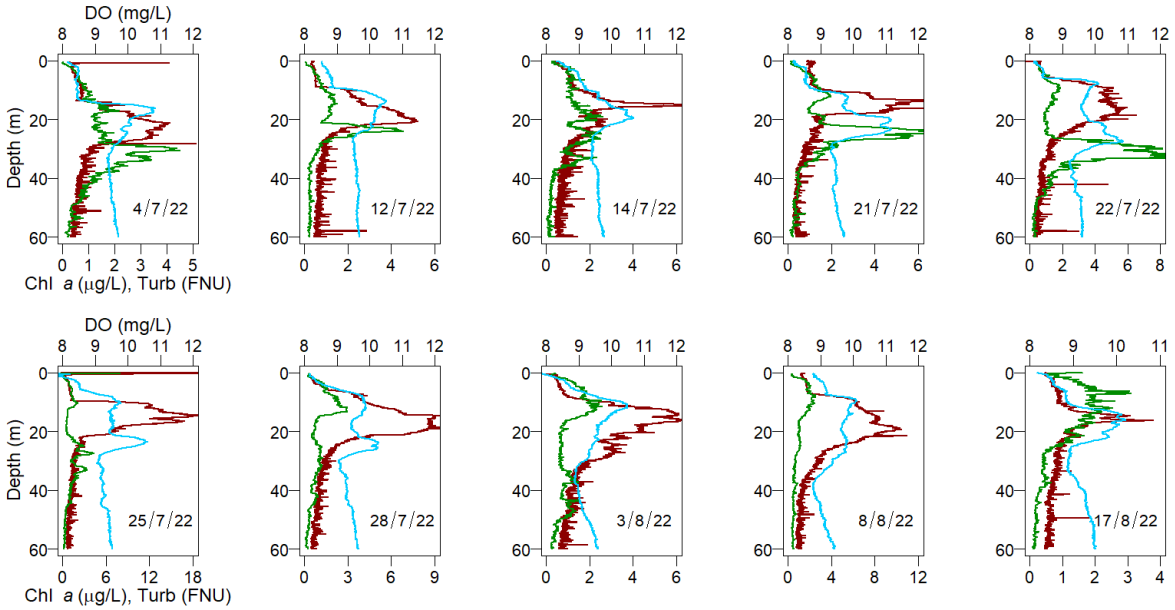

Fig. S2 Dissolved Oxygen (DO), Chlorophyll *a* (Chl *a*), and Turbidity (Turb) profile at the LéXPLORE station in 2022. The DO at the LéXPLORE station are likely inconclusive as both the primary production and the interflow generate DO local maxima in the water column. Blue, green, and red lines respectively indicate the DO, Chl *a,* and turbidity profiles.

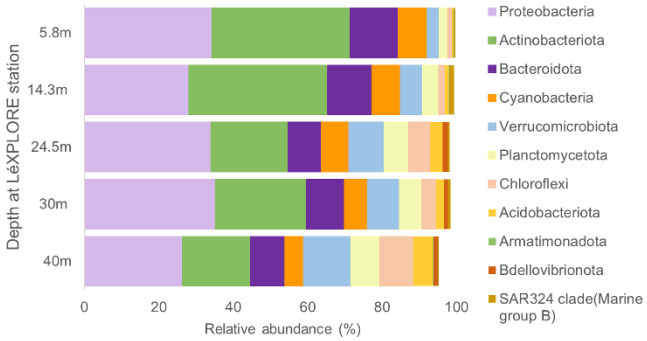

Fig. S3 Microbial community composition of the LéXPLORE water column in October 2022. The relative sequence abundance of the most abundant bacterial phylum using the Universal bacteria primer (Table S2) is shown here

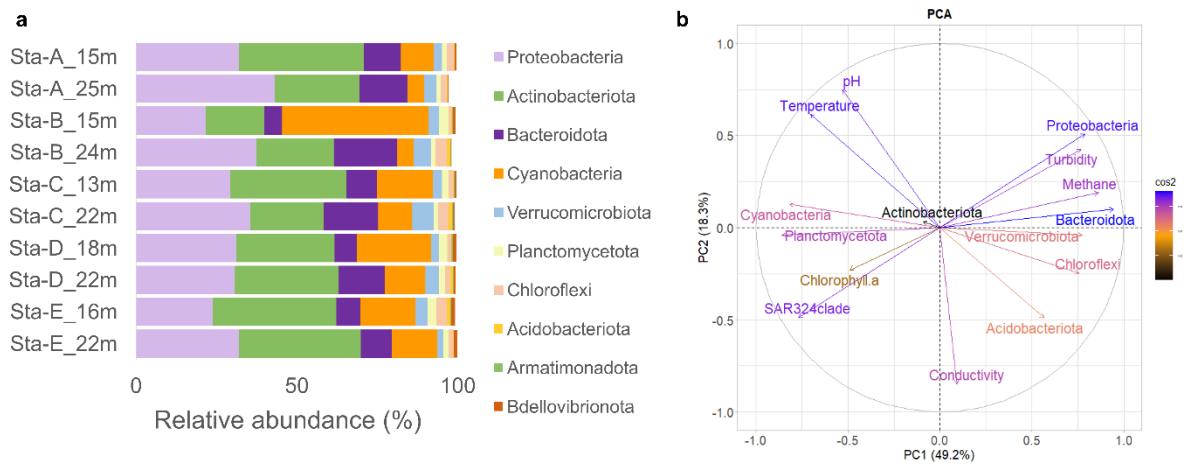

Fig. S4 Microbial community composition at the metalimnion of five stations in September 2022. (a) The relative sequence abundance of the most abundant bacterial phylum using the Universal bacteria primer (Table S2) is shown here. Among the sampling stations, Sta-E represents the microbial data for the LéXPLORE platform. **(b)** Principal component analysis of spatially distributed biogeochemical data is projected on orthogonal axes (PC1 and PC2) and the color indicates the weight of the contribution. Only variables contributing significantly to PCs are represented.

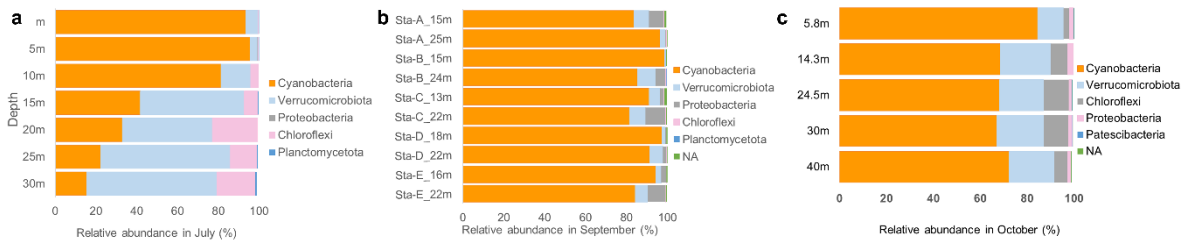

Fig. S5 Microbial community composition amplified with the Cyanobacteria-specific primer in July (a), September (b), and October (c) 2022 (from left to right). In July and October, the samples were collected from the LéXPLORE platform. In September, the microbial data for the LéXPLORE is represented as Sta-E. During the spatial distribution, the samples were collected from the metalimnion of StaA – StaE in September. The relative sequence abundance of bacterial phylum (Table S2) is shown here.

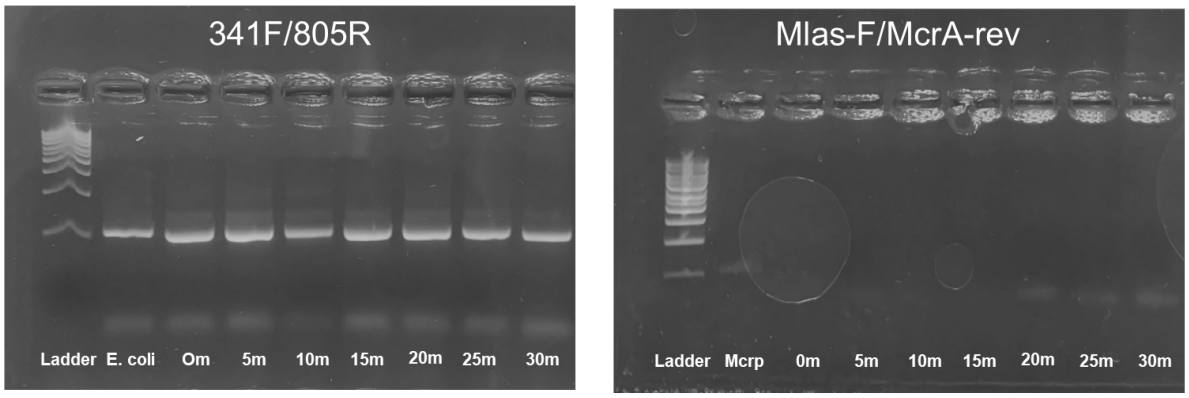

Fig. S6 Image of gel analysis for Bacteria and methanogens obtained from water samples collected in July 2022 at the LéXPLORE station. The polymerase chain reaction (PCR) products were amplified with the bacteria (341F/805R) and methanogens (Mlas-F/McrA-rev) subjected to denaturing gradient gel electrophoresis.

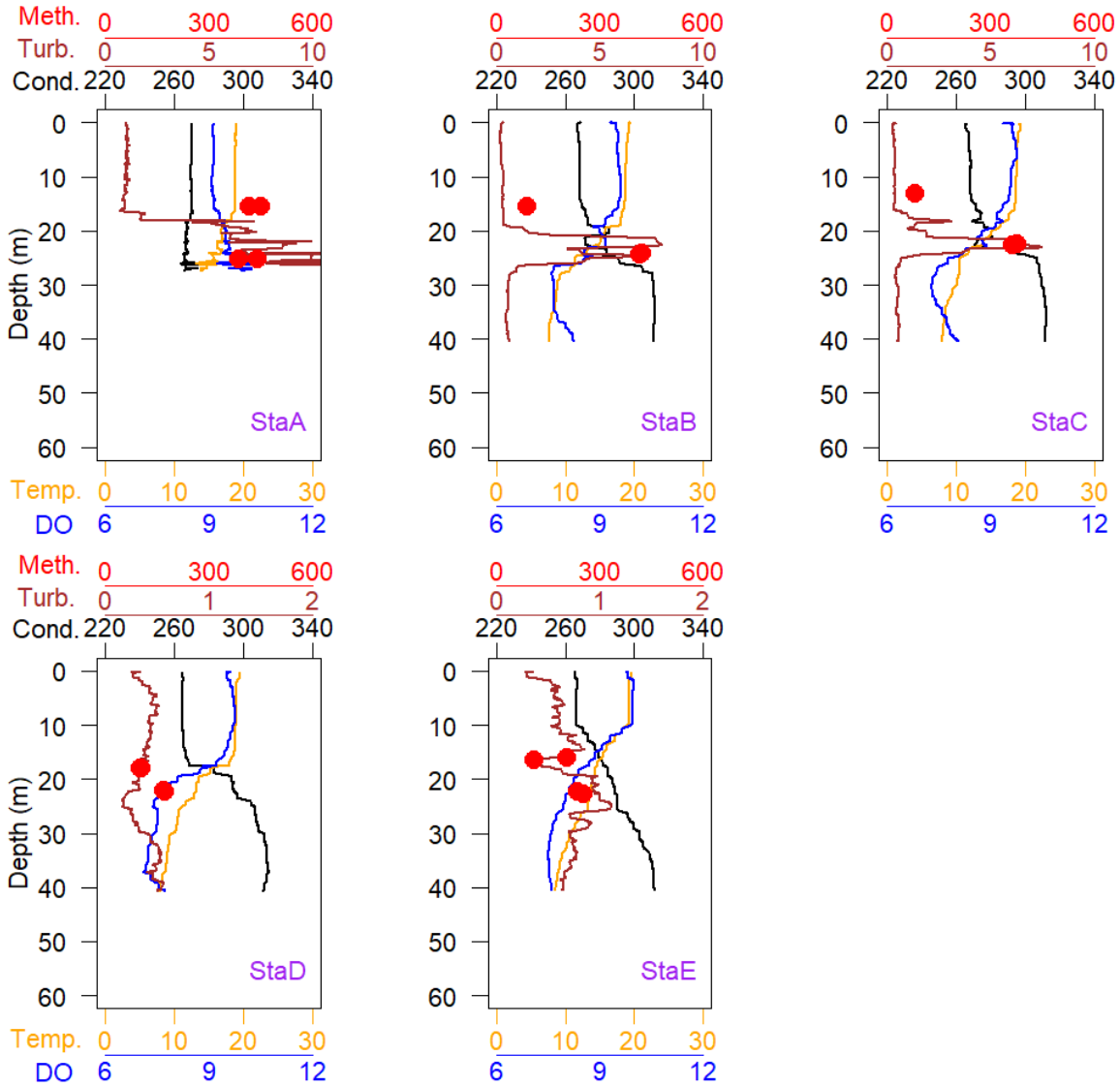

Fig. S7 Enviromental parameters during spatial methane distribution in five stations of Lake Geneva. Methane (Meth.; nM), Turbidity (Turb.; FNU), Conductivity (Cond.; µS/cm), Temperature (Temp.; °C), and Dissolved Oxygen (DO; mg/L) profile at the five sampling stations in September 2022. The Dissolved methane concentration used in Fig. 5 is shown using red dots for the two depths (between 13-25 m, two replications per depth) in each sampling station.

Table S1 Water and sediment sampling coordinates across Lake Geneva.

Date	Sampling Stations	Latitude N	Longitude E	Sample Type
July 22-23, 2021	1	46.396833	6.855567	Water for CH_4
	2	46.389633	6.857183	
	3	46.399917	6.85635	
	4	46.4005	6.852117	
	5	46.404133	6.853733	
	6	46.403267	6.848817	
	7	46.40525	6.847067	
	8	46.395183	6.824567	
	9	46.403517	6.8321	
	10	46.406633	6.83545	
	11	46.410617	6.838667	
	12	46.42315	6.856283	
	13	46.42875	6.853017	
	14	46.415667	6.833517	
	15	46.401833	6.819583	
March-September, 2021	Rhône River	46.349297	6.888556	
July-September, 2021	LéXPLORE	46.500369	6.660901	
July 27, 2022	LéXPLORE	46.500369	6.660901	Water for CH_4, Isotopoes, and microbes
September 23, 2022	StaA	46.396517	6.856369	
	StaB	46.405437	6.847079	
	StaC	46.410617	6.838667	
	StaD	46.441033	6.822529	
	StaE	46.500369	6.660901	
October 13, 2022	LéXPLORE	46.500369	6.660901	
July 26-27, 2023	LK1	46.40874	6.90895	Sediment for CH_4 Isotopes
	LK2	46.40998	6.88674	
	LK3	46.40394	6.86016	
	LK4	46.50039	6.66094	

Table S2 Primer pairs used in the community composition analysis.

Primer pairs	Target microbes	Forward	Reverse	Thermocycling conditions	Trimming parameters	References
341F, 805R	Bacteria	5'-CCTACGGGNGGCWGCAG-3'	5'-GACTACHVGGGTATCTAATCC-3'	95°C for 5min, 95°C for 40s, 55°C for 2min, 72°C for 1min, 72°C for 7 min	truncLen=c(270,250, maxN=0, maxEE=c(2,2), truncQ=2, rm.phix=TRUE	Klindworth et al. 2013
CYA106F, CYA781R	Cyanobacteria	5′-CGGACGGGTGAGTAACGCGTGA-3'	5′-GACTACTGGGGTATCTAATCCCATT-3'	94°C for 5min, 94°C for 1min, 60°C for 1min, 72°C for 1min, 72°C for 1.3min	truncLen=c(270,230), maxN=0, maxEE=c(2,2), truncQ=2, rm.phix=TRUE	Nübel et al. 1997
phnJF1, phnJR2	*Microbes having phnJ gene	5′-CSTATCTSGACGARCAGACSAA-3'	5′-TCGTCGGMGCCCTGRTCGA-3'	95°C for 5min, 95°C for 30s, 60°C for 30s, 72°C for 45s, 72°C for 1min	truncLen=c(150,140), maxN=0, maxEE=c(2,2), truncQ=2, rm.phix=TRUE	Morales et al. 2008
Mlas-F, McrA-rev	Methanogens	5'-GTGGTTMGGDTTCACMCARTA-3'	5'-CGTTCATBGCGTAGTTVGGRTAGT-3'	95°C for 5min, 95°C for 30s, 57°C for 1min, 72°C for 1.3min, 72°C for 5min	--	Steinberg and Regan 2008

*For the classification of *phnJ* gene, we obtained about 3948 of the C-P lyase protein sequences from the UniPlot (Protein sequence database). The corresponding mRNA (messenger RNA) entries were retrieved from the prokaryote section of the RefSeq (Reference sequence database) entries for each protein sequence using the tBLASTn (Translated Basic Local Alignment Search Tool) with a minimum expectation value of 1×10^{-8} and at least 90% sequence identity over the entire sequence following the protocol of Gertz et al 2006.

Table S3 Dissolved methane concentration (nM) in the Rhône water. The water samples were collected from the Rhône River (Rhône Porte du Scex station; lat/long: 46.349297/ 6.888556) in 2021.

Date	CH_4 (nM)
31/03/2021	37
10/05/2021	48.2
31/05/2021	21.9
05/07/2021	69.3
26/07/2021	38.2
30/09/2021	62.9

Table S4 Environmental variables that affect methane accumulation at the LéXPLORE station in 2021-2022. Linear regression was performed to identify the most impacting variable on the vertical methane profile revealing the significant relationship with dissolved oxygen (DO), temperature, conductivity, turbidity, and Chlorophyll *a*.

Metalinmetic depths (10m -25m)				
Response variable y	Explanatory variables x	*p*-value	*r*	r^2
CH_4 (nM) in both year 2021 and 2022 (df= 30)	Dissolved Oxygen (mg/L)	0.37	0.17	0.03
	Temperature	0.0005	0.58	0.33
	Chlorophyll *a*	0.43	-0.15	0.02
	Turbidity	8.091E-05	0.64	0.41
	Stability	3.847E-06	0.72	0.51
CH_4 (nM) in 2021 (df= 20)	Dissolved Oxygen (mg/L)	0.84	0.04	0.001
	Temperature	0.02	0.49	0.24
	Chlorophyll *a*	0.85	-0.04	0.001
	Turbidity	0.69	0.09	0.01
	Stability	0.13	0.34	0.11
CH_4 (nM) in 2022 (df= 8)	Dissolved Oxygen (mg/L)	0.09	0.56	0.32
	Temperature	0.03	0.68	0.46
	Chlorophyll *a*	0.82	-0.08	0.006
	Turbidity	0.03	0.69	0.47
	Stability	0.001	0.87	0.75

References for Supplementary information:

1. Klindworth, A., Pruesse, E., Schweer, T., Peplies, J., Quast, C., Horn, M., and F.O. Glöckner. 2013. Evaluation of general 16S ribosomal RNA gene PCR primers for classical and next-generation sequencing-based diversity studies. Nucleic acids research **41**: e1-e1. doi:10.1093/nar/gks808

2. Nübel, U., Garcia-Pichel, F., and G. Muyzer. 1997). PCR primers to amplify 16S rRNA genes from cyanobacteria. Applied and environmental microbiology, 63: 3327-3332. doi:10.1128/aem.63.8.3327-3332.1997

3. Morales, M. E., Allegrini, M., Basualdo, J., Villamil, M. B., and M. C. Zabaloy. 2020. Primer design to assess bacterial degradation of glyphosate and other phosphonates. Journal of microbiological methods **169**: 105814. doi:10.1016/j.mimet.2019.105814

4. Steinberg, L. M., and J. M. Regan. 2008. Phylogenetic comparison of the methanogenic communities from an acidic, oligotrophic fen and an anaerobic digester treating municipal wastewater sludge. Applied and environmental microbiology **74**: 6663-6671. doi:10.1128/AEM.00553-08

5. Gertz, E. M., Y.-K. Yu, R. Agarwala, A. A. Schäffer, and S. F. Altschul. 2006. Composition-based statistics and translated nucleotide searches: Improving the TBLASTN module of BLAST. BMC Biol **4**: 41. doi:10.1186/1741-7007-4-41